Available online at www.sciencedirect.com
SCIENCE DIRECT®
Nuclear Physics B 687 (2004) 76–100
NUCLEAR PHYSICS B
www.elsevier.com/locate/npe

# Propagators and running coupling from $SU(2)$ lattice gauge theory

J.C.R. Bloch [a], A. Cucchieri [b], K. Langfeld [c], T. Mendes [b]

[a] *DFG Research Center "Mathematics for Key Technologies", c/o Weierstrass Institute for Applied Analysis and Stochastics, Mohrenstrasse 39, D-10117 Berlin, Germany*
[b] *Instituto de Física de São Carlos, Universidade de São Paulo, C.P. 369, 13560-970 São Carlos, SP, Brazil*
[c] *Institut für Theoretische Physik, Universität Tübingen, D-72076 Tübingen, Germany*

Received 24 December 2003; received in revised form 13 February 2004; accepted 18 March 2004

**Abstract**

We perform numerical studies of the running coupling constant $\alpha_R(p^2)$ and of the gluon and ghost propagators for pure $SU(2)$ lattice gauge theory in the minimal Landau gauge. Different definitions of the gauge fields and different gauge-fixing procedures are used, respectively, for gaining better control over the approach to the continuum limit and for a better understanding of Gribov-copy effects. We find that the ghost–ghost–gluon vertex renormalization constant is finite in the continuum limit, confirming earlier results by all-order perturbation theory. In the low momentum regime, the gluon form factor is suppressed while the ghost form factor is divergent. Correspondingly, the ghost propagator diverges faster than $1/p^2$ and the gluon propagator appears to be finite. Precision data for the running coupling $\alpha_R(p^2)$ are obtained. These data are consistent with an IR fixed point given by $\lim_{p\to 0}\alpha_R(p^2) = 5(1)$.


*PACS:* 11.15.Ha; 12.38.Aw; 12.38.Lg; 14.70.Dj

*Keywords:* Gluon propagator; Ghost propagator; Running coupling constant; $SU(2)$ lattice gauge theory

## 1. Introduction

The non-perturbative study of non-Abelian gauge theories is of great importance for the determination of infrared (IR) properties such as color confinement and hadronization. These properties are encoded in the low momentum behavior of Yang–Mills Green's

*E-mail addresses:* attilio@if.sc.usp.br (A. Cucchieri), kurt.langfeld@uni-tuebingen.de (K. Langfeld).

0550-3213/$ – see front matter 
doi:10.1016/j.nuclphysb.2004.03.021

functions. Derived from these Green functions, the so-called (renormalized) running coupling constant "$\alpha_R(p^2)$" plays an important role for phenomenological studies and model building. While at large momentum the running coupling decreases logarithmically with momentum, it rapidly rises at the hadronic energy scale of several hundred MeVs thus signaling the breakdown of the perturbative approach. Non-perturbative studies of $\alpha_R(p^2)$ may be carried out analytically using the Dyson–Schwinger equations (DSEs) and numerically through lattice simulations.

Whereas the high momentum behavior of the running coupling is uniquely determined (to leading orders) and provided by perturbation theory, several definitions of the running coupling in the low momentum regime are possible. All of them match with the perturbative result at high energies. For example, the corrections to the Coulomb law of the static-quark potential may be used to define the running coupling [1,2]. Alternatively, the finite-size scaling has its imprint on the running coupling and may be used for a high-precision measurement of the coupling [3,4]. The approach adopted in [5–7] is based on extracting the running coupling directly from a vertex function. For a recent review of lattice calculations for $\alpha_R(p^2)$ see [8].

In order to obtain Green's functions for the fundamental degrees of freedom, gluons and quarks, gauge fixing is necessary. Despite being gauge-dependent, these Green functions play an important role for the phenomenological approach to hadron physics. Landau gauge is a convenient choice for gauge fixing for several reasons. First of all, it is a Lorentz-covariant gauge implying that 2-point functions only depend on the square of the momentum transfer. Secondly, the renormalization procedure is simplified since the ghost–ghost–gluon vertex renormalization constant $\tilde{Z}_1$ is finite, at least to all orders of perturbation theory. This result—obtained by Taylor [9]—is a particular feature of Landau gauge and allows another definition of the running coupling constant, which only requires the calculation of 2-point functions: let $F_R(p^2,\mu^2)$ and $J_R(p^2,\mu^2)$ denote the form factors (for a renormalization point $\mu$) of the gluon and the ghost propagator, respectively; the running coupling is then defined by

$$\alpha_R\big(p^2\big) = \alpha_R\big(\mu^2\big) F_R\big(p^2,\mu^2\big) J_R^2\big(p^2,\mu^2\big) \tag{1}$$

(see Section 2.7 below).

Due to its usefulness for the description of the physics of hadrons, the non-perturbative approach to low-energy Yang–Mills theory by means of the DSEs has attracted much interest over the last decade [10,11]. The coupled set of continuum DSEs for the renormalized gluon and ghost propagators in Landau gauge has been recently studied by several groups [12–25]. In all cases it was found that the gluon and ghost form factors satisfy simple scaling laws in the IR momentum range $p \ll 1$ GeV

$$F_R\big(p^2,\mu^2\big) \propto \big[p^2\big]^{\alpha}, \qquad J_R\big(p^2,\mu^2\big) \propto \big[p^2\big]^{\beta}, \tag{2}$$

where the remarkable sum rule holds for the IR exponents $\alpha$ and $\beta$:

$$\alpha + 2\beta = 0. \tag{3}$$

It is interesting that this result is rather independent of the truncation scheme under consideration. These exponents may be determined from lattice simulations, assuming the

parameterization $\alpha = 2\kappa$ and $\beta = -\kappa$. Note that for $\kappa > 0$ this implies a divergent ghost form factor $J_R(p^2, \mu^2)$ in the IR limit and a vanishing gluon form factor $F_R(p^2, \mu^2)$ in the same limit. Also, since the gluon propagator is given by $D(p^2) = F(p^2)/p^2$, one gets that $D(0)$ is infinite or finite, respectively, if $\kappa < 0.5$ or $\kappa \geqslant 0.5$. In the second case one has $D(0) = 0$ for $\kappa > 0.5$ and $D(0)$ finite and non-zero for $\kappa = 0.5$. The IR sum rule (3) also implies that the running coupling (defined in Eq. (61) below) develops a fixed point in the IR limit

$$\lim_{p\to 0} \alpha_R\big(p^2\big) = \alpha_c = \text{const.} \tag{4}$$

Note that this result is independent of the value of $\kappa$ as long as the IR sum rule (3) is satisfied.

The precise value of $\kappa$ as well as the fixed-point value $\alpha_c$ depend strongly on the truncation of the Dyson–Schwinger tower of equations. In fact, depending on the truncation, one finds $0.3 < \kappa < 1$ in the four-dimensional case [12,14–25]. These studies vary in their vertex ansatzes, angular approximations of the momentum loop integral, and on the tensor structure considered. In Ref. [17] a new class of truncation schemes has been introduced, which manifestly ensures the multiplicative renormalizability of the propagator solutions. In this truncation, although the exact values of $\kappa$ and $\alpha_c$ depend on the details of the truncation of the DSE tower, the value of $\alpha_c$ is constrained to

$$\frac{2\pi}{N_c} < \alpha_c < \frac{8\pi}{N_c} \tag{5}$$

for $SU(N_c)$.

An IR-finite gluon propagator [26–31] and an IR-divergent ghost form factor [30,31] are also obtained using numerical simulations in the minimal Landau gauge. The present numerical data for the ghost propagator indicate a value of $\kappa = -\beta$ smaller than 0.5, while for the gluon propagator it is still under debate if $\kappa = \alpha/2$ is equal to or larger than 0.5. In both cases large finite-size effects in the IR region make an exact determination of these exponents difficult. This is particularly evident in the gluon propagator case [26,27,29,32, 33], where one needs to go to very large lattices in order to have control over the infinite-volume extrapolation. Our present data are consistent with $\kappa$ of the order of 0.5 [34,35].

Let us stress that in the minimal Landau gauge, which is the gauge-fixing condition used in numerical simulations (see Section 2.3 below), the gauge-fixed configurations belong to the region of transverse configurations, for which the Faddeev–Popov operator is non-negative. This implies a rigorous inequality [36–38] for the Fourier components of the gluon field and a strong suppression of the (unrenormalized) gluon propagator in the IR limit. At the same time, the Euclidean probability gets concentrated near the border of this region, the so-called *first Gribov horizon*, implying the enhancement of the ghost propagator at small momenta [38]. A similar result was also obtained by Gribov in [39].

Taylor's finding is based upon the Faddeev–Popov quantization, thereby ignoring the effect of Gribov copies, which are certainly present in an intrinsically non-perturbative approach. The goal of the present paper is to confirm Taylor's result ($\tilde{Z}_1$ is finite to all orders of perturbation theory) by the non-perturbative approach provided by lattice simulations. In addition, a thorough study of the gluon and the ghost form factors is performed. A focal point is the IR limit of the running coupling constant. Support for the

existence of the fixed point is found, and a first estimate of $\alpha_c$ is provided from extensive lattice simulations. We present two sets of simulations, carried out, respectively, in São Carlos and in Tübingen, employing different definitions of the gauge fields and different gauge-fixing procedures. We believe that the comparison of these two formulations strengthens the significance of our findings.

The paper is organized as follows. In Section 2 we describe the lattice approach to Yang–Mills Green's functions. Section 3 contains the numerical setup for the simulations carried out in São Carlos and in Tübingen. In Section 4 we report our data for the gluon and ghost propagators and for the running coupling constant. Conclusions are left to the final section.

Preliminary results have been presented in [34,35,40,41].

## 2. The lattice approach to Green's functions

In this section we explain the two lattice setups used for the numerical evaluation of the gluon and ghost propagators. We also recall the definition of the running coupling constant considered in Ref. [12], which can be evaluated using these propagators.

### *2.1. Gluon field on the lattice*

The action $S$ of the continuum $SU(2)$ Yang–Mills theory is formulated in terms of the field strength

$$F^a_{\mu\nu}[A](x) = \partial_\mu A^a_\nu(x) - \partial_\nu A^a_\mu(x) + g_0 \epsilon^{abc} A^b_\mu(x) A^c_\nu(x) \tag{6}$$

and is given by

$$S = \frac{1}{4} \int d^4x \, F^a_{\mu\nu}[A](x) F^a_{\mu\nu}[A](x). \tag{7}$$

Here $g_0$ is the bare coupling constant and $A^a_\mu(x)$ is the continuum gauge field.

On the lattice the dynamical fields are $SU(2)$ matrices $U_\mu(x)$, which are associated with the links of the lattice, and the Wilson action is given by

$$S = \beta \sum_{x,\mu>\nu} 1 - \frac{1}{2} \operatorname{tr}_c P_{\mu\nu}(x), \tag{8}$$

where the plaquette is defined as

$$P_{\mu\nu}(x) = U_\mu(x) U_\nu(x + e_\mu) U^\dagger_\mu(x + e_\nu) U^\dagger_\nu(x) \tag{9}$$

and $e_\mu$ is a unit vector in the positive $\mu$ direction. (Note that the trace extends over color indices only.) The Wilson action is invariant under the gauge transformation

$$U^\Omega_\mu(x) = \Omega(x) U_\mu(x) \Omega^\dagger(x + e_\mu), \tag{10}$$

where $\Omega(x)$ are $SU(2)$ matrices. The link variables $U_\mu(x)$ may be expressed in terms of the continuum gauge field $A_\mu(x)$ by making use of the relation

$$U_\mu(x) = \exp\bigl[i a g_0 A^b_\mu(x) t^b\bigr], \tag{11}$$

where $a$ is the lattice spacing, $t^b = \sigma^b/2$ are the generators of the $SU(2)$ algebra and $\sigma^b$ are the Pauli matrices. One can check that in the naive continuum limit $a \to 0$ the Wilson action reproduces the continuum action in Eq. (7) if

$$\beta = \frac{4}{g_0^2} = \frac{1}{\pi\alpha_0}, \tag{12}$$

where $\alpha_0$ is the bare coupling constant (squared).

For the gauge group $SU(2)$, the link variables $U_\mu(x)$ can be given in terms of (real) four-vectors of unit length

$$U_\mu(x) = u_\mu^0(x)\mathbb{1} + i\vec{u}_\mu(x)\cdot\vec{\sigma}, \qquad \big[u_\mu^0(x)\big]^2 + \big[\vec{u}_\mu(x)\big]^2 = 1, \tag{13}$$

where $\mathbb{1}$ is a $2\times 2$ identity matrix. By defining the lattice gluon field $\mathcal{A}_\mu^b(x)$ as

$$\mathcal{A}_\mu^b(x) = \frac{U_\mu(x) - U_\mu^\dagger(x)}{2i} \tag{14}$$

one obtains

$$\mathcal{A}_\mu^b(x) = 2u_\mu^b(x) = ag_0 A_\mu^b(x) + \mathcal{O}\big(a^3\big) \tag{15}$$

in the naive continuum limit $a \to 0$. This definition has been used for the numerical simulations done in São Carlos.

Note that the gluon field $\mathcal{A}_\mu^b(x)$ defined above changes sign under a non-trivial center transformation $Z_2$ of the link fields $U_\mu(x) \to -U_\mu(x)$. Recently, another identification of the gluonic degrees of freedom in the lattice formulation was proposed [28]. In this case, one first notices that the gluon field in continuum Yang–Mills theories transforms under the *adjoint* representation of the $SU(2)$ color group, i.e.,

$$A_\mu^{a\prime}(x) = O^{ab}(x)A_\mu^b(x) + \frac{\epsilon^{aed}}{2}O^{ec}(x)\partial_\mu O^{dc}, \tag{16}$$

$$O^{ab}(x) = 2\,\mathrm{tr}_c\big[\Omega(x)t^a\Omega^\dagger(x)t^b\big], \tag{17}$$

where $\Omega(x) \in SU(2)$ is a gauge transformation of the fundamental quark field and $O^{ab}(x) \in SO(3)$. In view of the transformation properties in Eq. (16), one can identify the continuum gauge fields $A_\mu^a(x)$ with the algebra-valued fields of the adjoint representation

$$\mathcal{U}_\mu^{cd}(x) = \big\{\exp\big[ag_0 A_\mu^b(x)\hat{t}^b\big]\big\}^{cd}, \tag{18}$$

where $\hat{t}_{ac}^b = \epsilon^{abc}$ and the total anti-symmetric tensor $\epsilon^{abc}$ is the generator of the $SU(2)$ group in the adjoint representation. On the lattice, the adjoint links $\mathcal{U}_\mu^{ab}(x)$ are obtained from

$$\mathcal{U}_\mu^{cd}(x) = 2\,\mathrm{tr}_c\big[U_\mu(x)t^c U_\mu^\dagger(x)t^d\big] \tag{19}$$

and the gluon field $\mathcal{A}_\mu^a(x)$ is given by

$$\mathcal{A}_\mu^b(x) = 2u_\mu^0(x)u_\mu^b(x), \tag{20}$$

without summation over $\mu$ on the right-hand side. By expanding Eq. (18) in powers of the lattice spacing $a$ and by using Eqs. (13) and (19) one obtains

$$\mathcal{A}^b_\mu(x) = ag_0 A^b_\mu(x) + \mathcal{O}\big(a^3\big). \tag{21}$$

Clearly, the representation (20) is invariant under a non-trivial center transformation $U_\mu(x) \to -U_\mu(x)$. This discretization of the gluon field has been used for the simulations done in Tübingen.

It is well known that different discretizations of the gluon field lead to gluon propagators equivalent up to a trivial (multiplicative) renormalization [42–45]. Also, this proportionality constant between different discretizations of the gluon propagator may be (partially) explained as a tadpole renormalization [46,47]. We point out, however, that it is useful to disentangle the information carried by center elements and coset fields, defined above, when the vacuum energy is investigated. In particular, it was found that—in the continuum limit—the center elements provide a contribution to the gluon condensate [48, 49].

### *2.2. Tadpole improved gluon fields*

The relation between lattice and continuum gluon fields relies on the expansion (see Eq. (11))

$$U_\mu(x) = \mathbb{1} + iag_0 A^b_\mu(x) t^b + \cdots, \tag{22}$$

where the ellipses denote higher order terms in the bare coupling constant $g_0$. The artificial contributions of these higher order terms to loop integrals are called "tadpole" terms [50]. These terms are only suppressed by powers of $g_0^2$ and are generically large in simulations using moderate $\beta$ values.

In order to remove the tadpole contributions from the observable of interest one can redefine the relation between the link matrices and the continuum gluon field by using

$$U_\mu(x) = u_{0,L}\big[\mathbb{1} + iag_0 A^b_\mu(x) t^b + \cdots\big], \tag{23}$$

where $u_{0,L}$ is given by the "meanfield" value

$$u_{0,L} = \left\langle \frac{\mathrm{tr}_c}{2} U_\mu(x) \right\rangle \quad \text{(for arbitrary } \mu\text{)} \tag{24}$$

with the links $U_\mu(x)$ fixed to the Landau gauge. Equivalently, one can use [50] a gauge-invariant definition of the tadpole factor given by

$$u_{0,P} = \left[ \left\langle \frac{\mathrm{tr}_c}{2} P_{\mu\nu}(x) \right\rangle \right]^{1/4}, \tag{25}$$

where $P_{\mu\nu}(x)$ is the plaquette defined in Eq. (9). Thus, the use of tadpole improvement in the case of the standard definition of the lattice gluon field (15) gives

$$\mathcal{A}^b_\mu(x) = ag_0 A^b_\mu(x) + \mathcal{O}\big(a^3\big) = 2u^b_\mu(x)/u_{0,P}. \tag{26}$$

In the case of the coset definition (20) of the gauge fields, the tadpole factors are expressed in terms of the expectation values of the adjoint link and of the adjoint plaquette

and are given by

$$u_{0,L}^{\mathrm{ad}} = \left\langle \frac{\mathrm{tr}_c}{3} \mathcal{U}_\mu(x) \right\rangle, \tag{27}$$

$$u_{0,P}^{\mathrm{ad}} = \left[ \frac{1}{3} \langle \mathrm{tr}_c \, \mathcal{P}_{\mu\nu}(x) \rangle \right]^{1/4} = \left[ \frac{1}{3} \langle \left[ \mathrm{tr}_c \, P_{\mu\nu}(x) \right]^2 - 1 \rangle \right]^{1/4}. \tag{28}$$

Thus, the tadpole improved relation between the continuum gauge field $A_\mu^b(x)$ and the link matrices is given in this case by

$$\mathcal{A}_\mu^b(x) = a g_0 A_\mu^b(x) + \mathcal{O}(a^3) = 2 u_\mu^0(x) u_\mu^b(x) / u_{0,P}^{\mathrm{ad}}. \tag{29}$$

In the sections below we will stress the effect of tadpole improvement on the various quantities considered in this work.

### *2.3. Minimal Landau gauge*

The gluon and ghost propagators depend on the choice of the gauge. In order to maintain contact with the Dyson–Schwinger approach and the results presented in the Introduction, we consider the so-called minimal (lattice) Landau gauge. This gauge condition is imposed by minimizing the functional

$$S_{\mathrm{fix}}[\Omega] = -\sum_{x,\mu} \mathrm{tr}_c \, U_\mu^\Omega(x), \tag{30}$$

where $U_\mu^\Omega(x)$ is the gauge-transformed link (10). This minimizing condition corresponds to imposing the transversality condition

$$(\Delta \cdot \mathcal{A})^b(x) = \sum_\mu \mathcal{A}_\mu^b(x) - \mathcal{A}_\mu^b(x - e_\mu) = 0 \quad \forall b \text{ and } x, \tag{31}$$

which is the lattice formulation of the usual Landau gauge-fixing condition in the continuum. Let us notice that the condition (31) is exactly satisfied by the lattice gauge field only if the standard discretization (15) is considered, while for the discretization given in (20) the above result is valid up to discretization errors of order $a^2$. However, in both cases, the gauge-fixing condition (30) implies that the *continuum* Landau gauge-fixing condition $\partial \cdot A = 0$ is satisfied up to discretization errors of order $a^2$. In practice, we stop the gauge fixing when the average value of $[(\Delta \cdot \mathcal{A})^b(x)]^2$ is smaller than $10^{-12}$.

The minimizing condition (30) also implies that the Faddeev–Popov matrix is positive semi-definite. In particular, the space of gauge-fixed configurations $\{U_\mu^\Omega(x)\}$ lies within the first Gribov horizon, where the smallest (non-trivial) eigenvalue of the Faddeev–Popov operator is zero. It is well known that, in general, for a given lattice configuration $\{U_\mu(x)\}$, there are many possible gauge transformations $\Omega(x)$ that correspond to different local minima of the functional (30), i.e., there are *Gribov copies* inside the first Gribov horizon [36,37]. Thus, the minimizing condition given in Eq. (30) is not sufficient to find a unique representative on each gauge orbit. A possible solution to this problem is to restrict the configuration space of gauge-fixed fields $U_\mu^\Omega(x)$ to the so-called *fundamental modular region* [38], i.e., to consider for each configuration $\{U_\mu(x)\}$ the *absolute minimum* of

the functional (30). From the numerical point of view this is a highly non-trivial task, corresponding to finding the ground state of a spin-glass model [51]. On the other hand, if local minima are considered, one faces the problem that different numerical gauge-fixing algorithms yield different sets of local minima, i.e., they sample different configurations from the region delimited by the first Gribov horizon (see, for example, [44] and references therein). This implies that numerical results using gauge fixing could depend on the gauge-fixing algorithm, making their interpretation conceptually difficult.

In the simulations done in São Carlos, a stochastic overrelaxation algorithm [52–54] was used. The simulations done in Tübingen have employed the simulated annealing technique described in detail in Ref. [30]. The problem of Gribov copies was not considered in either case. Even though neither method is able to locate the *global* minimum of the gauge-fixing functional, i.e., to restrict the gauge-fixed configuration space to the fundamental modular region, a comparison of the propagators obtained using the two methods can provide an estimate of the bias (*Gribov noise*) introduced by the gauge-fixing procedure. From this comparison we have found that the data for the propagators are rather insensitive to the particular choice of gauge-fixing algorithm, suggesting that the influence of Gribov copies on the two propagators (if present) is at most of the order of magnitude of the numerical accuracy. For the gluon propagator this result is in agreement with previous studies in Landau gauge for the $SU(2)$ and $SU(3)$ groups in three [33] and four dimensions [31,44, 55]. A similar result has also been obtained for the gluon propagator in Coulomb gauge [56]. On the other hand, a previous study of the ghost propagator in $SU(2)$ Landau gauge [31] has shown a clear bias related to Gribov copies in the strong-coupling regime. In particular, data (in the IR region) obtained considering only absolute minima have been found to be systematically smaller than data obtained using local minima. This result—which has been recently confirmed in [57]—can be qualitatively explained. In fact, as said above, the smallest non-trivial eigenvalue $\lambda_{\min}$ of the Faddeev–Popov operator goes to zero as the first Gribov horizon is approached. At the same time, one expects that global minima (i.e., configurations belonging to the fundamental modular region) be "farther" away from the first Gribov horizon than local minima. Thus, the absolute minimum configuration should correspond to a value of $\lambda_{\min}$ larger—on average—than the value obtained in a generic relative minimum.[1] Since the ghost propagator is given by the inverse of the Faddeev–Popov matrix (see Section 2.5 below), this would imply a smaller ghost propagator (on average) at the absolute minimum, as observed in Refs. [31,57]. The analysis carried out in these references has shown that Gribov-copy effects are visible only for the smallest non-zero momentum on the lattice, at least for the lattice volumes considered, which are still relatively small. As explained below (see Section 4.3), in our analysis we have not considered the data points corresponding to the smallest momenta.

### *2.4. Gluon propagator*

The continuum gluon propagator in position space is given by

$$D^{ab}_{\mu\nu}(x-y) = \left\langle A^a_\mu(x) A^b_\nu(y) \right\rangle. \tag{32}$$

[1] This was checked numerically in Ref. [58].

Correspondingly, one can consider the (position space) lattice gluon propagator

$$\mathcal{D}^{ab}_{\mu\nu}(x-y) = \langle \mathcal{A}^a_\mu(x)\mathcal{A}^b_\nu(y)\rangle, \tag{33}$$

where $\mathcal{A}^a_\mu(x)$ is one of the lattice discretizations of the continuum gluon field discussed above (see Eqs. (15) and (20)). At the leading order $a$ these two quantities are related by

$$g_0^2 a^2 D^{ab}_{\mu\nu}(x-y) = \mathcal{D}^{ab}_{\mu\nu}(x-y)/u^2_{0,P}, \tag{34}$$

where $u_{0,P}$ is the tadpole factor given in Eq. (25) (respectively, Eq. (28)) when considering the lattice gluon field defined in Eq. (15) (respectively, Eq. (20)).

The lattice gluon propagator in momentum space is obtained by evaluating the Fourier transform

$$\mathcal{D}^{ab}_{\mu\nu}(\hat{p}) = \frac{1}{V}\sum_{x,y}\mathcal{D}^{ab}_{\mu\nu}(x-y)\exp\bigl[i\,\hat{p}\cdot(\hat{x}-\hat{y})\bigr], \qquad \hat{p}_\mu = \frac{2\pi n_\mu}{N_\mu}, \tag{35}$$

where $n_\mu$ labels the Matsubara modes in the $\mu$ direction, $N_\mu$ is the number of lattice points in the same direction, $x = \hat{x}a$, $y = \hat{y}a$ and $V$ is the lattice volume. In order to minimize discretization effects [59], we consider the gluon propagator as a function of the lattice momentum $p$ with components

$$p_\mu = 2\sin\left(\frac{\hat{p}_\mu}{2}\right). \tag{36}$$

It is also useful to introduce the lattice gluon form factor $\mathcal{F}(\hat{p}^2)$, defined as

$$\mathcal{D}(\hat{p}) = \frac{\mathcal{F}(\hat{p}^2)}{p^2}, \qquad \mathcal{D}(\hat{p}) = \frac{1}{9}\sum_{a,\mu}\mathcal{D}^{aa}_{\mu\mu}(\hat{p}), \tag{37}$$

which is a measure of the deviation of the full propagator from the free one. Note that, in Landau gauge, the propagator is diagonal in color space and transversal in Lorentz space. The transversality condition (31) implies [31] that $\mathcal{D}(0)$ is not given by $\mathcal{D}(\hat{p})$ at $\hat{p}=0$. In fact, for $\hat{p}=0$ the previous equation becomes $\mathcal{D}(0) = (1/12)\sum_{a,\mu}\mathcal{D}^{aa}_{\mu\mu}(0)$.

In order to evaluate numerically the gluon propagator in momentum space it is useful to employ the formula [31]

$$\mathcal{D}(\hat{p}) = \frac{1}{9V}\sum_{a,\mu}\left\langle\left[\sum_x \mathcal{A}^a_\mu(x)\cos(\hat{p}\cdot\hat{x})\right]^2 + \left[\sum_x \mathcal{A}^a_\mu(x)\sin(\hat{p}\cdot\hat{x})\right]^2\right\rangle. \tag{38}$$

In fact, by expanding the previous equation we obtain

$$\mathcal{D}(\hat{p}) = \frac{1}{9V}\sum_{a,\mu}\sum_{x,y}\langle \mathcal{A}^a_\mu(x)\mathcal{A}^a_\mu(y)\rangle\cos\bigl[\hat{p}\cdot(\hat{x}-\hat{y})\bigr], \tag{39}$$

which is directly related to Eq. (35).

One can also evaluate the form factor $F(\hat{p}^2)$ directly [28]. To this end we can consider, without any loss of generality, a momentum transfer parallel to the time direction $\hat{p} = (0,0,0,\hat{p}_4)$ and define

$$\Delta_t \mathcal{A}_\mu(x) = \mathcal{A}_\mu(x+e_4) - \mathcal{A}_\mu(x), \tag{40}$$

where $e_4$ is the unit vector in the time direction. The form factor is then obtained from

$$\mathcal{F}(\hat{p}^2) = \frac{1}{9V}\sum_{a,\mu}\left\langle\left[\sum_x \Delta_t \mathcal{A}^a_\mu(x)\cos(\hat{p}\cdot\hat{x})\right]^2 + \left[\sum_x \Delta_t \mathcal{A}^a_\mu(x)\sin(\hat{p}\cdot\hat{x})\right]^2\right\rangle. \quad (41)$$

By expanding the previous formula one can verify that the free part $1/p^2$ is canceled exactly. This strongly suppresses the statistical noise in the high-momentum regime. Here, we will present results that directly address the gluon propagator (38) and the gluon form factor (41), evaluated, respectively, in São Carlos and in Tübingen.

### 2.5. Ghost propagator

The ghost propagator $G^{ab}(\hat{p})$ is uniquely defined once the gauge-fixing functional (30) is specified. In fact, if we write the gauge-fixing matrix as

$$\Omega(x) = \exp\left[i\theta^a(x)t^a\right], \quad (42)$$

with $t^a$ defined as in Section 2.1, then the gauge-fixing functional can be expanded with respect to the angles $\theta^a(x)$ and, at any local minimum of $S_{\text{fix}}$, we obtain

$$S_{\text{fix}} = S_0 + \frac{1}{2}\sum_{x,y}\sum_{a,b}\theta^a(x)M^{ab}_{xy}\theta^b(y) + \mathcal{O}(\theta^3), \quad (43)$$

where $M^{ab}_{xy}$ is the so-called Faddeev–Popov operator. Note that the linear term in $\theta(x)$ is absent by virtue of the minimizing gauge-fixing condition (see Eqs. (30) and (31)). The expression of the Faddeev–Popov operator in terms of the gauge-fixed link variables can be found in [38, Eq. (B.18)]. Note that the matrix $M^{ab}_{xy}$ obtained in this way is a lattice discretization of the continuum Faddeev–Popov operator $(-\partial + A)\cdot\partial$ and that this discretization yields automatically the standard discretization $\mathcal{A}^b_\mu(x)$ for the gluon field given in Eq. (15).

The lattice ghost propagator $\mathcal{G}^{ab}(\hat{p})$ is provided by the inverse Faddeev–Popov operator $M^{ab}_{xy}$. Due to translation invariance, the lattice average of the inverse operator depends only on $(x-y)$. Thus, in momentum space we have

$$\mathcal{G}^{ab}(\hat{p}) = \frac{1}{V}\sum_{x,y}\left\langle\left(M^{-1}\right)^{ab}_{xy}\right\rangle\exp\left[-i\,\hat{p}\cdot(\hat{x}-\hat{y})\right]. \quad (44)$$

Since the matrix $M^{ab}_{xy}$ depends linearly on the link variables $U_\mu(x)$, tadpole improvement applied to the ghost propagator implies a rescaling

$$\mathcal{G}^{ab}(p) \to \mathcal{G}^{ab}(\hat{p})u_{0,P}. \quad (45)$$

Thus, at the leading order $a$ one has

$$a^2 G^{ab}(p) = \mathcal{G}^{ab}(\hat{p})u_{0,P}, \quad (46)$$

where $G^{ab}(p)$ is the continuum ghost propagator in momentum space.

The asymptotic behavior of the ghost propagator $G^{ab}(\hat{p})$ is known from perturbation theory: it decreases as $1/p^2$ with additional logarithmic corrections. The $1/p^2$ behavior is

inherited from the free-theory case. The non-trivial information on the ghost propagator is therefore encoded in the (continuum) form factor $J(\hat{p}^2)$, which is defined by

$$G^{ab}(\hat{p}) = \delta^{ab} G(\hat{p}) = \delta^{ab} \frac{J(\hat{p}^2)}{p^2}, \tag{47}$$

yielding the lattice form

$$\mathcal{G}^{ab}(\hat{p}) = \delta^{ab} \frac{\mathcal{J}(\hat{p}^2)}{p^2}. \tag{48}$$

Numerically, the lattice ghost propagator can be obtained by inverting the Faddeev–Popov matrix $M^{ab}_{xy}$. In the numerical simulations carried out in São Carlos this has been done using a conjugate-gradient algorithm. On the contrary, in the simulations in Tübingen the (lattice) ghost form factor $\mathcal{J}(\hat{p}^2)$ has been evaluated directly. To this end one can consider the following set of linear equations (for a given set of link variables $U$)

$$\sum_{y,b} M^{ab}_{xy}[U]\bar{u}^b(y) = n^a \big\{\cos\big[\hat{p}\cdot(\hat{x}-e_\mu)\big] - \cos[\hat{p}\cdot\hat{x}]\big\}, \tag{49}$$

$$\sum_{y,b} M^{ab}_{xy}[U]\bar{v}^b(y) = n^a \big\{\sin\big[\hat{p}\cdot(\hat{x}-e_\mu)\big] - \sin[\hat{p}\cdot\hat{x}]\big\}, \tag{50}$$

where $n^a$ is an arbitrary unit vector that specifies the components of the ghost propagator under investigation. We are considering momenta with a non-zero component only in the $\mu$ direction. In fact, by solving these equations for $\bar{u}^b(y)$ and $\bar{v}^b(y)$ and using trigonometric identities we find that the ghost form factor is given by

$$\begin{aligned}\mathcal{J}\big(\hat{p}^2\big) &= \frac{1}{V}\sum_{y}\Big\langle \big\{\cos\big[\hat{p}\cdot(\hat{y}-e_\mu)\big] - \cos[\hat{p}\cdot\hat{y}]\big\} n^b \bar{u}^b(y) \\ &\qquad + \big\{\sin\big[\hat{p}\cdot(\hat{y}-e_\mu)\big] - \sin[\hat{p}\cdot\hat{y}]\big\} n^b \bar{v}^b(y)\Big\rangle \qquad (51)\\ &= \frac{1}{V}\sum_{x,y}\sum_{a,b} n^b \big\langle \big(M^{-1}\big)^{ab}_{xy}\big\rangle n^a \left[4\sin^2\left(\frac{\hat{p}_\mu}{2}\right)\right]\cos\big[\hat{p}\cdot(\hat{x}-\hat{y})\big]. \qquad (52)\end{aligned}$$

Note that, with our choice of momenta, the lattice momentum squared is given by $p^2 = 4\sin^2(\hat{p}_\mu/2)$, implying that the free part $1/p^2$ of the ghost propagator exactly cancels out and we are left with the form factor $\mathcal{J}(\hat{p}^2)$. The set of equations (49)–(50) has been solved using a bi-conjugate gradient method for matrix inversion.

### *2.6. Renormalization*

Renormalization of Yang–Mills theories in four dimensions implies that the bare coupling acquires a dependence on the ultraviolet (UV) cutoff $\Lambda_{\mathrm{UV}}$ given by

$$\alpha_0 \to \alpha_0(\Lambda_{\mathrm{UV}}/\Lambda_{\mathrm{scale}}). \tag{53}$$

Thereby, the bare coupling constant is no longer the theory's parameter. The Yang–Mills scale parameter $\Lambda_{\mathrm{scale}}$ takes over the role of the only parameter of the theory. In the context

of (quenched) lattice-gauge-theory simulations of the string tension $\sigma$ is widely used as the generic low-energy scale. In this case, the cutoff dependence of the bare coupling is implicitly given by the $\beta$ dependence of $\sigma a^2(\beta)$ where $\beta$ is related to the bare coupling in (12) and $\Lambda_{\mathrm{UV}} = \pi/a(\beta)$. In Section 3.3 we will derive this relation from lattice data (obtained in Ref. [60]).

In addition, wave-function renormalization constants develop a dependence on $\Lambda_{\mathrm{UV}}/\Lambda_{\mathrm{scale}}$. The lattice bare form factors of the previous subsections, $\mathcal{F}_B$ and $\mathcal{J}_B$, are related to their continuum analogues (for very large $\beta$) by

$$F_B = \mathcal{F}_B \frac{\beta}{4u_{0,P}^2}, \qquad J_B = \mathcal{J}_B u_{0,P}. \tag{54}$$

These form factors depend on the momentum $p^2$ and on the UV cutoff $\Lambda_{\mathrm{UV}}$ (given in units of the string tension) or, equivalently, on the lattice coupling $\beta$ (see Section 4.3 below). Thus, we can write

$$\mathcal{F}_B = \mathcal{F}_B\big(p^2, \beta\big), \qquad \mathcal{J}_B = \mathcal{J}_B\big(p^2, \beta\big). \tag{55}$$

The renormalized form factors are obtained upon multiplicative renormalization

$$F_R\big(p^2, \mu^2\big) = Z_3^{-1}(\beta, \mu) F_B\big(p^2, \beta\big), \tag{56}$$

$$J_R\big(p^2, \mu^2\big) = \tilde{Z}_3^{-1}(\beta, \mu) J_B\big(p^2, \beta\big), \tag{57}$$

using the renormalization conditions

$$F_R\big(\mu^2, \mu^2\big) = 1, \qquad J_R\big(\mu^2, \mu^2\big) = 1. \tag{58}$$

(Notice that tadpole renormalization does not affect the calculation of $F_R$, $J_R$ but may be useful for the determination of the renormalization constants $Z_3$, $\tilde{Z}_3$.)

Clearly, similar relations hold also for the bare and renormalized gluon and ghost propagators. In practice, the multiplicative renormalizability of the theory implies that a rescaling of the data for each $\beta$ value (independently of the lattice momentum) is sufficient to let the form factors $\mathcal{F}_B(p^2, \beta)$ and $\mathcal{J}_B(p^2, \beta)$—or equivalently the corresponding propagators—fall on top of a single curve describing the momentum dependence of the corresponding renormalized quantity.

### *2.7. Running coupling constant*

Of great importance for phenomenological purposes is the running coupling strength $\alpha_R(p^2)$ considered in Ref. [12]. In particular, this strength enters directly the quark DSE and can be interpreted as an effective interaction strength between quarks [61]. This running coupling strength is a renormalization-group-invariant combination of the gluon and ghost form factors. In order to derive this combination we can start with the definition of the ghost–ghost–gluon vertex renormalized coupling strength

$$\alpha_R\big(\mu^2\big) = \frac{Z_3(\beta, \mu)\tilde{Z}_3^2(\beta, \mu)}{\tilde{Z}_1^2(\beta, \mu)} \alpha_0(\Lambda_{\mathrm{UV}}), \tag{59}$$

where $\tilde{Z}_1(\beta,\mu)$ is the ghost–ghost–gluon vertex renormalization constant. In lattice simulations, the UV-cutoff is related to $\beta$ by $\Lambda_{\rm UV} = \pi/a(\beta)$, where $a$ is the lattice spacing. Using Eqs. (56) and (57) we can express the renormalization constants $Z_3(\beta,\mu)$ and $\tilde{Z}_3(\beta,\mu)$ in terms of the bare and renormalized form factors yielding

$$\alpha_R\big(\mu^2\big)F_R\big(p^2,\mu^2\big)J_R^2\big(p^2,\mu^2\big) = \frac{\alpha_0(\Lambda_{\rm UV})}{\tilde{Z}_1^2(\beta,\mu)}F_B\big(p^2,\beta\big)J_B^2\big(p^2,\beta\big). \tag{60}$$

Note that the left-hand side of this relation is finite and independent of $\beta$ by construction and that the right-hand side depends on the renormalization scale $\mu$ only through the ghost–ghost–gluon vertex renormalization constant $\tilde{Z}_1(\beta,\mu)$. It was found more than twenty years ago by Taylor [9] that (in the continuum) $\tilde{Z}_1$ is finite, independent of $\mu$, at least to all orders of perturbation theory. This finding will be confirmed by our lattice studies below. In this case, the right-hand side of Eq. (60) is thus independent of $\mu$. Then, by choosing $\mu = \sqrt{p^2}$ and using the renormalization conditions (58), we find the final expression for the running coupling strength, i.e.,

$$\alpha_R\big(p^2\big) = \alpha_R\big(\mu^2\big)F_R\big(p^2,\mu^2\big)J_R^2\big(p^2,\mu^2\big). \tag{61}$$

Finally, let us notice that Eqs. (34) and (46) imply that tadpole renormalization does not affect the renormalized coupling defined above.

## 3. Details of the numerical simulations

### 3.1. Setup

All our simulations used the standard Wilson action for $SU(2)$ lattice gauge theory in four dimensions with periodic boundary conditions. In order to check finite-volume effects and verify scaling we consider several values of $\beta$ and of the lattice volumes $V = N_s^3 \times N_t$. The dependence of the lattice spacing on $\beta$ can be inferred from a calculation of the string tension $\sigma$ in lattice units. Here, we will use the data for $\sigma a^2$ reported in Ref. [60] and a linear interpolation of the logarithm of these data where needed.[2] A value of the lattice spacing in physical units was obtained using the value $\sigma = [440\ \text{MeV}]^2$ for the string tension. We used $N_{\rm conf}$ independent configurations for the numerical evaluation of the propagators.

Computations in São Carlos were performed on the PC cluster at the IFSC-USP (the system has 16 nodes with 866 MHz Pentium III CPU and 256 MB RAM memory). All runs in São Carlos started with a random gauge configuration and for thermalization we use a *hybrid overrelaxed* (HOR) algorithm. The total computer time used for the runs was about 50 days on the full PC cluster. In Table 1 we report the parameters used for the simulations in São Carlos. For each $\beta$ value three different lattice volumes were considered, i.e., $V = 14^4$, $20^4$ and $26^4$. For the lattice volume $V = 14^4$ (respectively, $V = 20^4$ and $26^4$) and for each $\beta$ value we produced $N_{\rm conf} = 500$ (respectively, 150 and 50) configurations.

[2] For $\beta = 2.15$ an extrapolation of these data was necessary in order to obtain $\sigma a^2$.

Table 1
Simulation parameters of the runs in São Carlos. Data from Ref. [60] were used to obtain the lattice spacing in units of the string tension. Error bars (in parentheses) come from propagation of errors and indicate one standard deviation on the last significant digit. The lattice volumes $V$ and the number of configurations $N_{\text{conf}}$ considered are discussed in the text

| $\beta$ | 2.2 | 2.3 | 2.4 | 2.5 | 2.6 | 2.7 | 2.8 |
|---|---|---|---|---|---|---|---|
| $\sigma a^2$ | 0.220(9) | 0.136(2) | 0.071(1) | 0.0363(3) | 0.018(1) | 0.0103(2) | 0.0055(3) |

Table 2
Simulation parameters of the runs in Tübingen. Data from Ref. [60] were used to obtain the lattice spacing in units of the string tension

| $\beta$ | 2.15 | 2.2 | 2.3 | 2.375 | 2.45 | 2.525 |
|---|---|---|---|---|---|---|
| $\sigma a^2$ | 0.280(13) | 0.220(9) | 0.136(2) | 0.083(2) | 0.0507(8) | 0.0307(5) |
| $N_s^3 N_t$ | $16^3 \times 32$ | $16^3 \times 32$ | $16^3 \times 32$ | $16^3 \times 32$ | $16^3 \times 32$ | $16^3 \times 32$ |
| $N_{\text{conf}}$ | 200 | 200 | 200 | 200 | 200 | 200 |

Table 3
Differences between the São Carlos and the Tübingen numerical approach

| | São Carlos | Tübingen |
|---|---|---|
| Definition of gauge fields | fundamental representation | adjoint representation |
| Gauge fixing | iterative stoch. overrelaxation | simulated annealing |
| Number of lattice points | finite-size control | fixed |

Computations in Tübingen were carried out at the local PC cluster where 4–12 nodes (1 Ghz Athlon) were used. The simulation parameters for the runs in Tübingen are listed in Table 2.

Table 3 lists the differences between the São Carlos and the Tübingen approach. Reconstructing the continuum gauge field from the link fields in different manners (compare Eq. (15) with Eq. (20)) provides insight into the discretization errors. Employing different gauge-fixing algorithms points out the effect of the Gribov ambiguities on the propagators.

### *3.2. Determination of renormalization constants*

In order to obtain the renormalized propagators and form factors, one needs to evaluate the renormalization constants $Z_3^{-1}(\beta,\mu)$ and $\tilde{Z}_3^{-1}(\beta,\mu)$ defined in Eqs. (56) and (57), respectively. Multiplicative renormalizability implies that one can "collapse" data obtained at different $\beta$ on a single curve. This can be done by using the matching technique described in detail in Ref. [62, Section V.B.2], For instance, for the gluon form factor this is equivalent to considering the quantity

$$F_R\big(p^2,\mu^2\big) = Z_3^{-1}(\beta,\mu) F_B\big(\beta,p^2\big), \tag{62}$$

where the factor $Z_3^{-1}(\beta,\mu)$ for each $\beta$ is obtained from the matching technique. The renormalization point, i.e., the $\mu$-dependence, comes into play when the "single" curve

is rescaled to satisfy the condition

$$F_R(\mu^2, \mu^2) = 1. \tag{63}$$

The same procedure is applied to the ghost form factor. For our analysis we considered a renormalization scale of $\mu = 3$ GeV.

For the São Carlos data we checked for finite-size effects before applying the matching technique.[3] In particular, by comparing data at different lattice sizes and same $\beta$ value, we find (for each $\beta$) a range of momenta for which the data are free from finite-volume corrections. We then perform the matching using data for these momenta and $V = 26^4$.

### 3.3. Asymptotic scaling

As said in Section 2.6, the cutoff dependence of the bare coupling is implicitly given by $\sigma a^2(\beta)$. Thereby, the string tension $\sigma$ serves as the fundamental energy scale.

In principle, perturbation theory predicts the $\beta$ dependence of $\sigma a^2$ for the regime $a \ll 1/\sqrt{\sigma}$. In practice, large deviations of the measured function $\sigma a^2(\beta)$ from the perturbative scaling are observed in the scaling region, which corresponds to the interval $\beta \in [2.15, 2.8]$ in our case. Clearly, the relation between the "measured" values for $\sigma a^2$ and perturbation theory is highly important for a careful extrapolation of the lattice data to continuum physics. One goal of the present paper is to present this relation.

For this purpose, we perform a large $\beta$ expansion of the lattice spacing in units of the string tension, i.e.,

$$\ln(\sigma a^2) = -\frac{4\pi^2}{\beta_0}\beta + \frac{2\beta_1}{\beta_0^2}\ln\left(\frac{4\pi^2}{\beta_0}\beta\right) + \frac{4\pi^2}{\beta_0}\frac{d}{\beta} + c. \tag{64}$$

The first two terms on the rhs of (64) are in accordance with 2-loop perturbation theory. The term $d/\beta$ represents higher order effects and the term $c$ is a dimensionless scale factor to the string tension. Parameters $c$ and $d$ are determined by fitting the formula (64) to the lattice data reported in Ref. [60]. Using only data for $\beta \geqslant 2.3$ we obtain

$$c = 4.38(9), \qquad d = 1.66(4), \qquad \chi^2/\text{d.o.f.} = 0.62. \tag{65}$$

The corresponding fit is shown in Fig. 1. It appears that the truncation of the series (64) at the $1/\beta$ level reproduces the measured values to high accuracy.

In order to illustrate the impact of the $d$-term correction in (64) on the estimate of Yang–Mills scale parameters, we briefly consider the lattice scale parameter $\Lambda_{\text{lat}}$. This parameter is implicitly defined at the 2-loop level by considering [50]

$$\alpha_{\text{lat}}^{-1} = \frac{\beta_0}{4\pi}\ln\left(\frac{1}{a^2\Lambda_{\text{lat}}^2}\right) + \frac{\beta_1}{2\pi\beta_0}\ln\left[\ln\left(\frac{1}{a^2\Lambda_{\text{lat}}^2}\right)\right], \tag{66}$$

where for the $SU(N)$ gauge group

$$\beta_0 = \frac{11}{3}N, \qquad \beta_1 = \frac{17}{3}N^2, \qquad \alpha_{\text{lat}}^{-1} = \frac{2\pi}{N}\beta. \tag{67}$$

[3] For more details see [33, Section III].

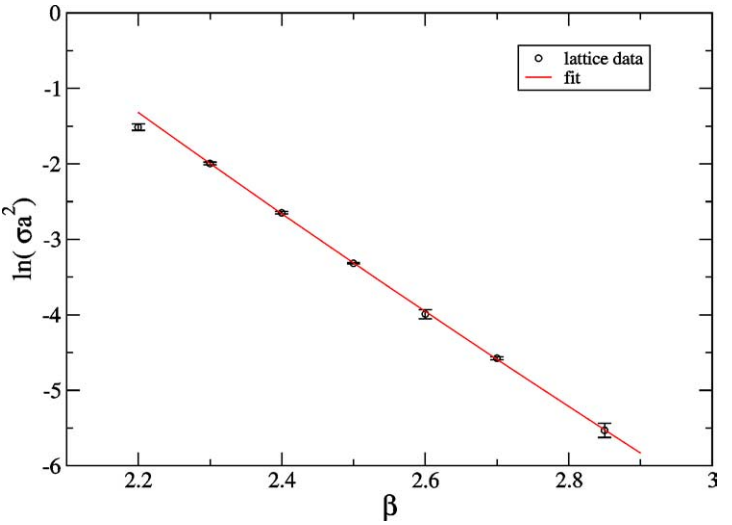


Fig. 1. The string tension in units of the lattice spacing: lattice data from [60] and the fit using Eq. (64).

Inverting Eq. (66) consistently up to 2-loop perturbation theory yields

$$\ln\bigl(a^2\Lambda_{\rm lat}^2\bigr) \doteq -\frac{4\pi}{\beta_0}\alpha_{\rm lat}^{-1} + \frac{2\beta_1}{\beta_0^2}\ln\biggl(\frac{4\pi}{\beta_0}\alpha_{\rm lat}^{-1}\biggr). \tag{68}$$

Then, using $\alpha_{\rm lat}^{-1} = \pi\beta$ from Eq. (67) and eliminating $a$ by subtracting Eq. (64) from the latter equation we find

$$\ln\biggl(\frac{\Lambda_{\rm lat}^2}{\sigma}\biggr) = \lim_{\beta\to\infty}\biggl[-c - \frac{4\pi^2}{\beta_0}\frac{d}{\beta}\biggr]. \tag{69}$$

Thus, if we extrapolate to the continuum limit $\beta \to \infty$ we obtain

$$\Lambda_{\rm lat} = e^{-c/2}\sqrt{\sigma} = 0.112(5)\sqrt{\sigma}. \tag{70}$$

Using the value $\sigma = [440\ \text{MeV}]^2$ one gets $\Lambda_{\rm lat} = 49(2)$ MeV. If one instead of the limit in (69) assumes that the asymptotic scaling regime is reached for, e.g., $\beta = 2.5$, one gets $\Lambda_{\rm lat} = 0.0188(8)\sqrt{\sigma}$. This is the order of magnitude familiar from the literature. Hence, for a scaling analysis of lattice results employing $\beta \in [2.15, 2.8]$ the irrelevant term of order $1/\beta$ is still important.

## 4. Results

### *4.1. Renormalization constants $Z_3$, $\tilde{Z}_3$ and $\tilde{Z}_1$*

Let us firstly focus on the renormalization constants $Z_3$ and $\tilde{Z}_3$. As outlined in Section 3.2, these constants are obtained from "matching" the lattice data from simulations

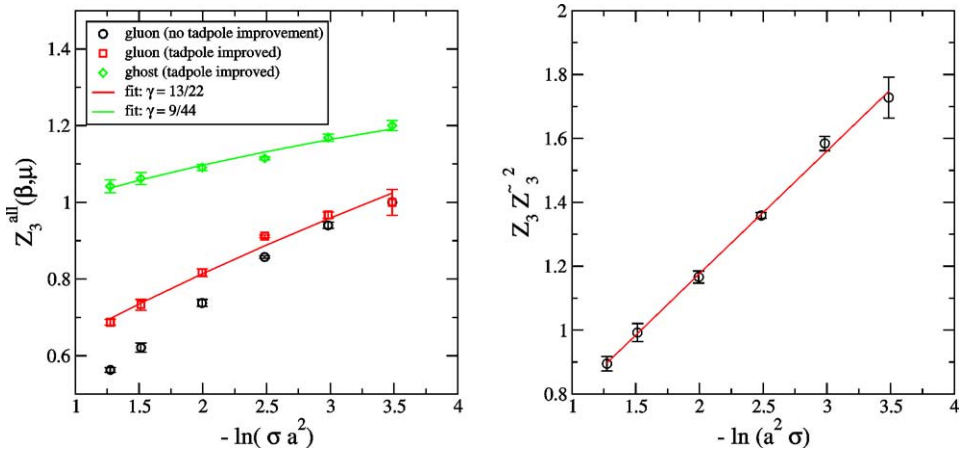


Fig. 2. The gluon and ghost renormalization constants, $Z_3(\beta,\mu)$ and $\tilde{Z}_3(\beta,\mu)$, for $\mu = 3$ GeV (left panel), $y$ axis is arbitrarily scaled. The cutoff dependence of $Z_3\tilde{Z}_3^2$ (right panel) is consistent with a finite $\tilde{Z}_1$ (see Eqs. (74), (75)). Figures corresponding to the Tübingen data only.

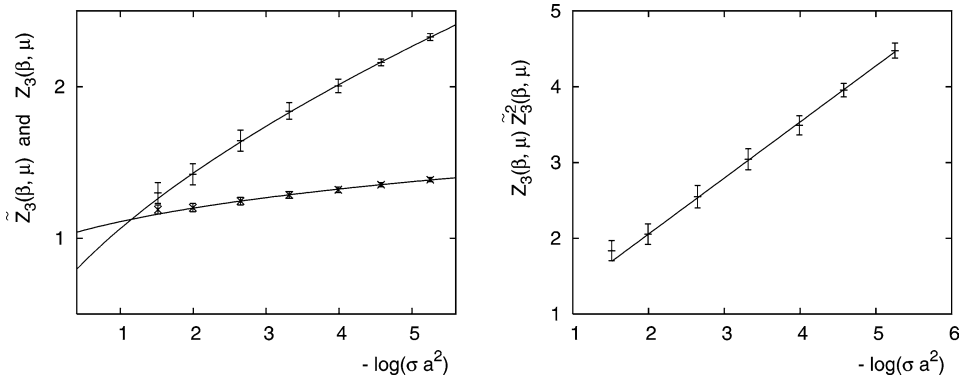


Fig. 3. The analogue of Fig. 2, for the São Carlos data. The fits shown on the left-hand side for the gluon (upper curve) and ghost (lower curve) renormalization constants are done with $\gamma$ as a free parameter. All fits neglect the leftmost data point.

using different $\beta$ values. Figs. 2 and 3 show the cutoff dependence of these constants, respectively, for the Tübingen and São Carlos sets of data.

Using the results above, we can check that our data are consistent with the predictions from perturbation theory. For large enough UV cutoff, one expects that the 1-loop behavior is recovered, i.e.,

$$Z_3(\beta,\mu),\ \tilde{Z}_3(\beta,\mu) \approx b\big[-\ln\big(\sigma a^2\big)+\omega\big]^{\gamma}. \tag{71}$$

Table 4
Expectation value of the adjoint plaquette (28) used for the tadpole improvement of the gluon fields derived from the adjoint representation

| $\beta$ | 2.15 | 2.2 | 2.3 | 2.375 | 2.45 | 2.525 |
|---|---|---|---|---|---|---|
| $u_{0,P}^{\mathrm{ad}}$ | 0.225(42) | 0.241(43) | 0.274(45) | 0.297(46) | 0.317(46) | 0.336(47) |

If only small lattice spacings are considered, $\omega$ is related to the ratio between the string tension and the Yang–Mills scale parameter at 1-loop level

$$\omega = \ln \frac{\pi^2 \sigma}{\Lambda_{\text{1-loop}}^2}. \tag{72}$$

Here, we treat $\omega$ as a fit parameter and explore a range of lattice spacings where one would already expect significant deviations from the 1-loop behavior. As shown in Figs. 2 and 3 (left panel), a good consistency with the known anomalous dimensions is observed.

For the Tübingen data, we find that $\omega \approx 1.13$ is a good choice for reproducing the data for $Z_3$ and $\tilde{Z}_3$ simultaneously. It turns out that within the $\beta$ range explored in the Tübingen runs, tadpole improvement has a minor effect on the anomalous dimension. The adjoint plaquette used for the tadpole improvement (see Eq. (34)) employing the adjoint representation is listed in Table 4.

For the São Carlos data we have performed the fits with $\gamma$ as a free parameter, leaving out the data point with $\beta = 2.2$ (i.e., the leftmost point in Fig. 3). We obtain the following values for the gluon and ghost cases

$$\gamma_{\text{gluon}} = 0.60(5) \quad \text{and} \quad \gamma_{\text{ghost}} = 0.32(7). \tag{73}$$

We see that the values are, respectively, consistent with $13/22 \approx 0.59$ and $9/44 \approx 0.20$ within error bars (but notice that there is a discrepancy of almost two standard deviations for $\gamma_{\text{ghost}}$). In this case we have not succeeded in finding a value of $\omega$ describing the behaviors for $Z_3$ and $\tilde{Z}_3$ simultaneously.

In order to interpret the product of ghost and gluon form factors as the running coupling strength (see Section 2.7), it is of great importance that the ghost–ghost–gluon vertex renormalization constant $\tilde{Z}_1$ be finite in the continuum limit. For detecting the UV behavior of $\tilde{Z}_1$, let us investigate the product

$$Z_3(\beta,\mu)\tilde{Z}_3^2(\beta,\mu) = \frac{\alpha_R(\mu^2)}{\alpha_0(\Lambda_{\text{UV}})}\tilde{Z}_1^2(\beta,\mu), \tag{74}$$

where (59) was used. The left-hand side of the latter equation can be directly obtained from the numerical result for the renormalization constants $Z_3(\beta,\mu)$ and $\tilde{Z}_3(\beta,\mu)$. Note that for large UV cutoff, one finds

$$\frac{1}{\alpha_0(\Lambda_{\text{UV}})} \propto \ln \frac{\Lambda_{\text{UV}}^2}{\Lambda_{\text{1-loop}}^2} = -\ln\bigl(\sigma a^2\bigr) + \text{const}, \tag{75}$$

where the constant comprises cutoff (and therefore $\beta$) independent terms. The crucial point is that if the product $Z_3(\beta,\mu)\tilde{Z}_3^2(\beta,\mu)$ rises linearly with $-\ln(\sigma a^2)$ the additional factor

$\tilde{Z}_1^2(\beta,\mu)$ must be finite in the continuum limit (since the renormalized coupling $\alpha_R(\mu^2)$ is assumed finite). Our numerical findings for $Z_3(\beta,\mu)\tilde{Z}_3^2(\beta,\mu)$ are also shown in Figs. 2 and 3 (right panel). The data nicely support Taylor's findings, i.e., $\tilde{Z}_1$ is cutoff- and therefore $\mu$-independent.

### *4.2. The running coupling constant*

Once it is established that $\tilde{Z}_1$ is finite, the momentum dependence of the running coupling constant can be simply derived from the product (61)

$$\alpha_R\big(p^2\big) = \alpha_R\big(\mu^2\big) F_R\big(p^2,\mu^2\big) J_R^2\big(p^2,\mu^2\big). \tag{76}$$

The overall normalization factor can be obtained by comparing the lattice data with the well-known perturbative result, which is valid at high momentum. Here, we compare with the 2-loop expression, which is known to be independent of the renormalization prescription, i.e.,

$$\alpha_{2\text{-loop}}\big(x = p^2/\Lambda_{2\text{-loop}}^2\big) = \frac{4\pi}{\beta_0 \ln x}\left\{1 - \frac{2\beta_1}{\beta_0^2}\frac{\ln(\ln x)}{\ln x}\right\}, \tag{77}$$

with $\beta_0$ and $\beta_1$ given in Eq. (67). In order to obtain $\Lambda_{2\text{-loop}}$ and to fix the overall factor, we fitted $\alpha_R(\mu)F_R(p^2,\mu^2)J_R^2(p^2,\mu^2)$ to the 2-loop running coupling $\alpha_{2\text{-loop}}(p)$ where only momenta $p \geqslant p_M$ were taken into account. Fitting parameters were $\alpha_R(\mu)$ and the 2-loop perturbative scale $\Lambda_{2\text{-loop}}$. Starting from a very low value $p_M$ we fit these parameters while gradually increasing $p_M$. For small values of $p_M$, we observe that the functional form of (77) tries to incorporate genuine non-perturbative effects by adjusting $\Lambda_{2\text{-loop}}$, thus, introducing a spurious $p_M$ dependence to $\Lambda_{2\text{-loop}}$. However, a plateau is reached for the Tübingen data at $p_M \approx 2$ GeV indicating that the data are well reproduced by the 2-loop formula in this regime. We find in this case that

$$\Lambda_{2\text{-loop}} = 0.95(15)\ \text{GeV}. \tag{78}$$

For the São Carlos data we have cut the data at $p_M \approx 2.5$ GeV, which corresponds to a large drop in the $\chi^2$/d.o.f. of the fit. (This also corresponds to reaching a relatively good plateau for $\Lambda_{2\text{-loop}}$ obtained from the fit.) We obtain the value $\Lambda_{2\text{-loop}} = 1.2(1)$ GeV. The two values are consistent within error bars.

Our final results for the running coupling constant are presented in Fig. 4. In the IR region, the two data sets show a clear departure from the perturbative behavior and suggest a finite value $\alpha_c$ for the running coupling constant at zero momentum. We estimate $\alpha_c = 5(1)$. This value is in agreement with our previous fits for $\alpha_R(p^2)$ [34,35], and is consistent with the DSE result of Ref. [25], $\alpha_c \approx 5.2$, using $\kappa = 0.5$ as input.

### *4.3. Gluon and ghost form factors*

Fig. 5 shows the Tübingen data for the gluon and the ghost form factors. The error bars comprise statistical errors only. It turns out that one observes an additional scattering of the data points which is not of statistical origin. This additional systematic noise is

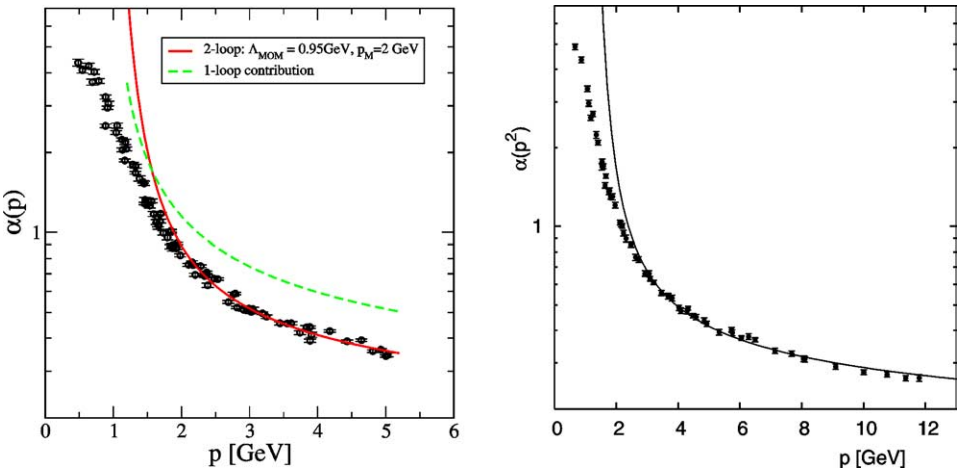


Fig. 4. The running coupling in comparison with the results from perturbation theory: Tübingen data (left panel) and São Carlos data (right panel). The momentum cutoff is $p_M = 2$ GeV in the former case and $p_M = 2.5$ GeV in the latter.

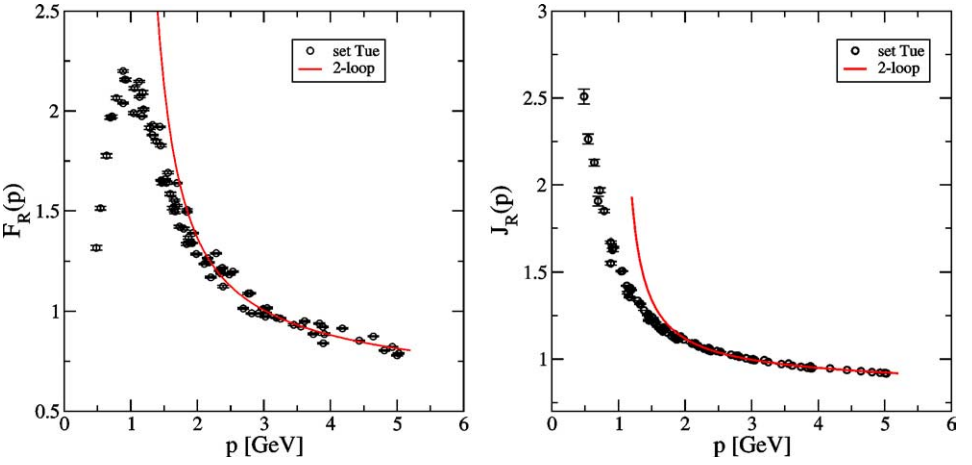


Fig. 5. The gluon form factor $F_R(p)$ and the ghost form factor $J_R(p)$ as a function of the momentum transfer $p$ (Tübingen data).

pronounced when simulated annealing is used for gauge fixing and it afflicts especially the small momentum range. We attribute this error to the residual uncertainty of gauge fixing (Gribov noise). In particular, since the simulated annealing is capable of hopping from one local minimum to the other, the algorithm is sensitive to the large-scale structure of the minimizing functional. This hopping then produces a non-Gaussian noise which is underestimated when one uses the standard Gaussian error propagation. For this reason, we dropped the first three momentum points from the Tübingen data sets.

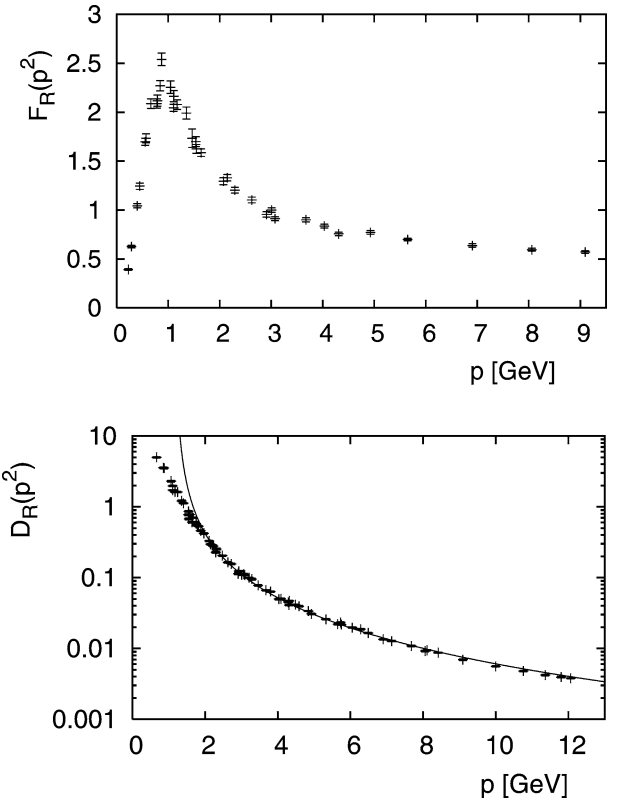


Fig. 6. The gluon form factor $F_R(p)$ (above) and the gluon propagator $D_R(p)$ (below) as a function of the momentum transfer $p$ (São Carlos data). Note the logarithmic scale in the second plot. Fit of gluon propagator using the analogue of Eq. (79) has been done for momenta $p \geqslant 2$ GeV and with $\Lambda = 1.2$ GeV.

In Figs. 6 and 7 we report the rescaled São Carlos data for the renormalized gluon (respectively, ghost) form factor and the data for the corresponding propagators. We stress that in the gluon case finite-size effects depend on whether we consider the full propagator or the form factor. In fact, for the propagator these effects are larger in the IR region, while for the form factor the effects are larger in the UV limit (due to the multiplication by $p^2$). Thus, the ranges of momenta (for each $\beta$) considered for the plots are different in the two cases. Nevertheless, the matching factors obtained are in agreement. The difference in finite-size effects between propagator and form factor is less pronounced when considering the ghost propagator.

At sufficiently high momentum $p \geqslant p_M$ (we found in Section 4.2 that $p_M \approx 2$ GeV is an acceptable choice), the momentum dependence of the renormalized form factors should be given by the formula

$$F_R\big(p^2,\mu^2\big), J_R\big(p^2,\mu^2\big) \approx d_2(\mu)\left[\alpha_{2\text{-loop}}\left(\frac{p^2}{\Lambda^2_{2\text{-loop}}}\right)\right]^{\gamma}\left[1+\bar{\gamma}\alpha_{2\text{-loop}}\left(\frac{p^2}{\Lambda^2_{2\text{-loop}}}\right)\right], \tag{79}$$

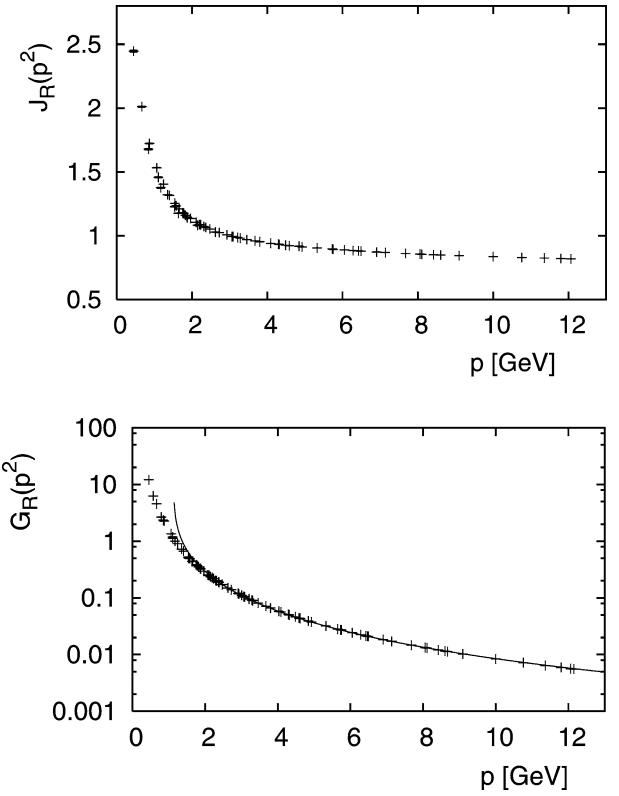


Fig. 7. The ghost form factor $J_R(p)$ (above) and the ghost propagator $G_R(p)$ (below) as a function of the momentum transfer $p$ (São Carlos data). Note the logarithmic scale in the second plot. Fit of ghost propagator using the analogue of Eq. (79) has been done for momenta $p \geqslant 2$ GeV and with $\Lambda = 1.2$ GeV.

where $\gamma$ is the leading-order anomalous dimension of the gluon (respectively, ghost) propagator, given by $\gamma = 13/22$ (respectively, $\gamma = 9/44$). The parameter $\bar{\gamma}$ stems from the next to leading order to the anomalous dimension and is scheme-dependent. At least in the $\overline{\text{MS}}$ scheme, this parameter is small. Furthermore, Eq. (79) can be derived from the renormalization-group equation using the 2-loop scaling functions $\beta(g_R)$ and $\gamma_A(g_R)$. Hence, (79) originates from the resummation of an infinite set of 2-loop diagrams and, e.g., comprises the so-called "leading logs".

Using the Tübingen data set, $p_M = 2$ GeV and $\Lambda_{\text{2-loop}} = 950$ MeV, we fitted $\bar{\gamma}$ to the gluon and ghost data, respectively. We find that these parameters are, indeed, small, i.e.,

$$\bar{\gamma}_{\text{gluon}} = -0.036(18), \qquad \bar{\gamma}_{\text{ghost}} = 0.011(10). \tag{80}$$

Although the errors on these parameters are rather large, we find it encouraging that the parameters appear with opposite signs. In the case that the product of form factors $F_R(p^2)J_R^2(p^2)$ is, indeed, renormalization group invariant, one would expect that

$$\bar{\gamma}_{\text{gluon}} + 2\bar{\gamma}_{\text{ghost}} = 0. \tag{81}$$

It is clear from the Figs. 2 and 5 that the high momentum tail is well reproduced by (79).

For the São Carlos data we have found that a cut at $p_M = 2\text{GeV}$ corresponds to a large drop in the $\chi^2$/d.o.f. of the fits, both for the gluon and for the ghost cases. We start by fitting the leading-order term only (i.e., ignoring $\bar{\gamma}$). We get

$$\Lambda_{2\text{-loop}} = 1.19(4) \quad \text{and} \quad \Lambda_{2\text{-loop}} = 1.13(2), \tag{82}$$

respectively, from the fits of the gluon and of the ghost propagator. These values are consistent with the result $\Lambda_{2\text{-loop}} = 1.2(1)$, obtained in the previous section. We then fix this value for $\Lambda_{2\text{-loop}}$ and perform fits with $\bar{\gamma}$ as a free parameter. We obtain a good description of the data (see Figs. 6 and 7), with values for $\bar{\gamma}$ even consistent with zero.

As can be seen from our plots, the gluon form factor is suppressed in the low momentum regime, while the ghost form factor is divergent. Correspondingly, the ghost propagator diverges faster than $1/p^2$ and the gluon propagator appears to be finite. As mentioned in the introduction, an IR-finite gluon propagator [26–31] and an IR-divergent ghost form factor [30,31] were obtained before by separate studies.

A quantitative analysis of the IR behavior for the propagators—including the evaluation of the exponent $\kappa$ mentioned in the introduction—was already presented in Refs. [34, 35]. More thorough such analyses will be presented separately for the two sets of data in Refs. [63,64].

## 5. Conclusions

For the first time, evidence from extensive lattice simulations is provided that the ghost–ghost–gluon vertex renormalization constant $\tilde{Z}_1$ is, indeed, finite in continuum field theory (as found by Taylor using all orders perturbation theory). Also, our result is probably not affected by Gribov ambiguities, since $\tilde{Z}_1$ is obtained using data in the UV limit. It therefore appears that the Gribov ambiguities (in the lattice approach and the Faddeev–Popov quantization) do not afflict the renormalization of the vertex.

Also, we performed a thorough study of the gluon and the ghost form factors. Our data favor the scenario of an IR finite (or even vanishing) gluon propagator while the ghost form factor is singular in the IR limit.

Finally, we have obtained the running coupling constant over a wide range of momenta using the data for gluon and ghost form factors. Our data are consistent with the existence of an IR fixed point $\alpha_c = 5(1)$. Note that this value is inside the interval given by the DSE expression (5).

We stress that we compared our results for two slightly different lattice formulations, obtaining consistent results in all cases considered.

## Acknowledgements

J.C.R.B.'s contribution was funded by the Deutsche Forschungsgemeinschaft (Project No. SCHM 1342/3-1) and by the DFG Research Center "Mathematics for Key Technologies" (FZT 86) in Berlin. K.L. greatly acknowledges the stimulating atmosphere and the

hospitality of the Institute for Theoretical Physics, University of Karlsruhe where parts of the project were performed. The research of A.C. and T.M. is supported by FAPESP (Project No. 00/05047-5). We thank C.S. Fischer for helpful comments on the manuscript.

## References

[1] C. Michael, Phys. Lett. B 283 (1992) 103, hep-lat/9205010.
[2] G.S. Bali, K. Schilling, Phys. Rev. D 47 (1993) 661, hep-lat/9208028.
[3] M. Luscher, R. Sommer, P. Weisz, U. Wolff, Nucl. Phys. B 413 (1994) 481, hep-lat/9309005.
[4] G.M. de Divitiis, R. Frezzotti, M. Guagnelli, R. Petronzio, Nucl. Phys. B 422 (1994) 382, hep-lat/9312085.
[5] C. Parrinello, Phys. Rev. D 50 (1994) 4247, hep-lat/9405024.
[6] J. Skullerud, A. Kizilersu, JHEP 0209 (2002) 013, hep-ph/0205318.
[7] S. Furui, H. Nakajima, in: Wien 2000, Quark Confinement and the Hadron Spectrum, 2000, p. 275, hep-lat/0012017.
[8] A. Cucchieri, in: Proceedings of Hadron Physics 2002, World Scientific, Singapore, 2003, p. 161, hep-lat/0209076.
[9] J.C. Taylor, Nucl. Phys. B 33 (1971) 436.
[10] C.D. Roberts, S.M. Schmidt, Prog. Part. Nucl. Phys. 45 (2000) S1, nucl-th/0005064.
[11] R. Alkofer, L. von Smekal, Phys. Rep. 353 (2001) 281, hep-ph/0007355.
[12] L. von Smekal, R. Alkofer, A. Hauck, Phys. Rev. Lett. 79 (1997) 3591, hep-ph/9705242.
[13] L. von Smekal, A. Hauck, R. Alkofer, Ann. Phys. 267 (1998) 1, hep-ph/9707327;
L. von Smekal, A. Hauck, R. Alkofer, Ann. Phys. 269 (1998) 182, Erratum.
[14] D. Atkinson, J.C.R. Bloch, Phys. Rev. D 58 (1998) 094036, hep-ph/9712459.
[15] D. Atkinson, J.C.R. Bloch, Mod. Phys. Lett. A 13 (1998) 1055, hep-ph/9802239.
[16] D. Zwanziger, Phys. Rev. D 65 (2002) 094039, hep-th/0109224.
[17] J.C.R. Bloch, Phys. Rev. D 64 (2001) 116011, hep-ph/0106031.
[18] C. Lerche, Diploma thesis, University Erlangen-Nuremberg, June 2001 (in German).
[19] C. Lerche, L. von Smekal, Phys. Rev. D 65 (2002) 125006, hep-ph/0202194.
[20] C.S. Fischer, R. Alkofer, Phys. Lett. B 536 (2002) 177, hep-ph/0202202.
[21] C.S. Fischer, R. Alkofer, H. Reinhardt, Phys. Rev. D 65 (2002) 094008, hep-ph/0202195.
[22] R. Alkofer, W. Detmold, C.S. Fischer, P. Maris, hep-ph/0309077.
[23] R. Alkofer, W. Detmold, C.S. Fischer, P. Maris, hep-ph/0309078.
[24] D. Zwanziger, Phys. Rev. D 67 (2003) 105001, hep-th/0206053.
[25] J.C.R. Bloch, Few Body Syst. 33 (2003) 111, hep-ph/0303125.
[26] A. Cucchieri, Phys. Lett. B 422 (1998) 233, hep-lat/9709015.
[27] A. Cucchieri, Phys. Rev. D 60 (1999) 034508, hep-lat/9902023.
[28] K. Langfeld, H. Reinhardt, J. Gattnar, Nucl. Phys. B 621 (2002) 131, hep-ph/0107141.
[29] F.D. Bonnet, et al., Phys. Rev. D 64 (2001) 034501, hep-lat/0101013.
[30] H. Suman, K. Schilling, Phys. Lett. B 373 (1996) 314, hep-lat/9512003.
[31] A. Cucchieri, Nucl. Phys. B 508 (1997) 353, hep-lat/9705005.
[32] A. Cucchieri, D. Zwanziger, Phys. Lett. B 524 (2002) 123, hep-lat/0012024.
[33] A. Cucchieri, T. Mendes, A.R. Taurines, Phys. Rev. D 67 (2003) 091502, hep-lat/0302022.
[34] J.C.R. Bloch, A. Cucchieri, K. Langfeld, T. Mendes, Nucl. Phys. B (Proc. Suppl.) 119 (2003) 736, hep-lat/0209040.
[35] K. Langfeld, J.C.R. Bloch, J. Gattnar, H. Reinhardt, A. Cucchieri, T. Mendes, in: Gargnano 2002, Quark Confinement and the Hadron Spectrum, 2003, p. 297, hep-th/0209173.
[36] D. Zwanziger, Phys. Lett. B 257 (1991) 168.
[37] D. Zwanziger, Nucl. Phys. B 364 (1991) 127.
[38] D. Zwanziger, Nucl. Phys. B 412 (1994) 657.
[39] V.N. Gribov, Nucl. Phys. B 139 (1978) 1.
[40] A. Cucchieri, T. Mendes, D. Zwanziger, Nucl. Phys. B (Proc. Suppl.) 106 (2002) 697, hep-lat/0110188.
[41] K. Langfeld, hep-lat/0204025.

[42] L. Giusti, M.L. Paciello, S. Petrarca, B. Taglienti, M. Testa, Phys. Lett. B 432 (1998) 196, hep-lat/9803021.
[43] A. Cucchieri, F. Karsch, Nucl. Phys. B (Proc. Suppl.) 83 (2000) 357, hep-lat/9909011.
[44] L. Giusti, M.L. Paciello, C. Parrinello, S. Petrarca, B. Taglienti, Int. J. Mod. Phys. A 16 (2001) 3487, hep-lat/0104012.
[45] I.L. Bogolubsky, V.K. Mitrjushkin, hep-lat/0204006.
[46] A. Cucchieri, T. Mendes, in: Strong and Electroweak Matter, Copenhagen 1998, 1999, p. 324, hep-lat/9902024.
[47] A. Cucchieri, in: Understanding Deconfinement in QCD, Trento 1999, 1999, p. 202, hep-lat/9908050.
[48] K. Langfeld, E.M. Ilgenfritz, H. Reinhardt, G. Shin, Nucl. Phys. B (Proc. Suppl.) 106 (2002) 501, hep-lat/0110024.
[49] K. Langfeld, E.M. Ilgenfritz, H. Reinhardt, A. Schafke, Nucl. Phys. B (Proc. Suppl.) 106 (2002) 658, hep-lat/0110055.
[50] G.P. Lepage, P.B. Mackenzie, Phys. Rev. D 48 (1993) 2250, hep-lat/9209022.
[51] E. Marinari, C. Parrinello, R. Ricci, Nucl. Phys. B 362 (1991) 487.
[52] A. Cucchieri, T. Mendes, Nucl. Phys. B 471 (1996) 263, hep-lat/9511020.
[53] A. Cucchieri, T. Mendes, Nucl. Phys. B (Proc. Suppl.) 53 (1997) 811, hep-lat/9608051.
[54] A. Cucchieri, T. Mendes, Comput. Phys. Commun. 154 (2003) 1, hep-lat/0301019.
[55] J.E. Mandula, Phys. Rep. 315 (1999) 273.
[56] A. Cucchieri, D. Zwanziger, Phys. Rev. D 65 (2002) 014001, hep-lat/0008026.
[57] T.D. Bakeev, et al., hep-lat/0311041.
[58] A. Cucchieri, Nucl. Phys. B 521 (1998) 365, hep-lat/9711024.
[59] P. Marenzoni, G. Martinelli, N. Stella, Nucl. Phys. B 455 (1995) 339, hep-lat/9410011.
[60] J. Fingberg, U.M. Heller, F. Karsch, Nucl. Phys. B 392 (1993) 493, hep-lat/9208012.
[61] J.C.R. Bloch, Phys. Rev. D 66 (2002) 034032, hep-ph/0202073.
[62] D.B. Leinweber, et al., Phys. Rev. D 60 (1999) 094507, hep-lat/9811027;
D.B. Leinweber, et al., Phys. Rev. D 61 (2000) 079901, Erratum.
[63] J.C.R. Bloch, K. Langfeld, in preparation.
[64] A. Cucchieri, T. Mendes, in preparation.